Tellus (2003), 55B, 901–913
Printed in UK. All rights reserved

TELLUS
ISSN 0280–6509

Atmospheric response to Saharan dust deduced from ECMWF reanalysis (ERA) temperature increments

By P. KISHCHA[1]*, P. ALPERT[1], J. BARKAN[1], I. KIRCHNER[2] and B. MACHENHAUER[3], [1]*Department of Geophysics and Planetary Sciences, Tel Aviv University, Tel-Aviv, 69978, Israel;* [2]*Max-Planck-Institute for Meteorology, Hamburg, 20146, Germany;* [3]*Danish Meteorological Institute, Copenhagen, DK-2100, Denmark*

(Manuscript received 21 May 2002; in final form 20 February 2003)

ABSTRACT

This study focuses on the atmospheric temperature response to dust deduced from a new source of data–the European Reanalysis (ERA) increments. These increments are the systematic errors of global climate models, generated in the reanalysis procedure. The model errors result not only from the lack of desert dust but also from a complex combination of many kinds of model errors. Over the Sahara desert the lack of dust radiative effect is believed to be a predominant model defect which should significantly affect the increments. This dust effect was examined by considering correlation between the increments and remotely sensed dust. Comparisons were made between April temporal variations of the ERA analysis increments and the variations of the Total Ozone Mapping Spectrometer aerosol index (AI) between 1979 and 1993. The distinctive structure was identified in the distribution of correlation composed of three nested areas with high positive correlation (>0.5), low correlation and high negative correlation (< -0.5). The innermost positive correlation area (PCA) is a large area near the center of the Sahara desert. For some local maxima inside this area the correlation even exceeds 0.8. The outermost negative correlation area (NCA) is not uniform. It consists of some areas over the eastern and western parts of North Africa with a relatively small amount of dust. Inside those areas both positive and negative high correlations exist at pressure levels ranging from 850 to 700 hPa, with the peak values near 775 hPa. Dust-forced heating (cooling) inside the PCA (NCA) is accompanied by changes in the static instability of the atmosphere above the dust layer. The reanalysis data of the European Center for Medium Range Weather Forecast (ECMWF) suggest that the PCA (NCA) corresponds mainly to anticyclonic (cyclonic) flow, negative (positive) vorticity and downward (upward) airflow. These findings are associated with the interaction between dust-forced heating/cooling and atmospheric circulation. This paper contributes to a better understanding of dust radiative processes missed in the model.

1. Introduction

The role of aerosols in climate has become a matter of extensive scientific attention. Recent research suggests that their role may be very important in the alteration of the radiation balance in the atmosphere due to the absorption and scattering of solar and thermal radiation (Kaufman et al., 2002; Miller and Tegen, 1998). Nevertheless, most state-of–the-art climate models do not yet include these aerosol effects, due to the dearth of necessary information about the temporal and spatial distribution of aerosol. An important observation severely lacking is the vertical structure of dust plumes; this structure is essential for the radiation forcing calculations. It was shown (Hamonou et al., 1999; Gobbi et al., 2000) that the vertical structure for the African dust transport over the Atlantic Ocean is different from the Mediterranean dust transport. In accordance with Kaufman et al. (2001), the extent of dust absorption of solar radiation is not fully known due to the accuracy limitations of *in situ* measurements. These previous models, which included the dust generation, showed some essential discrepancies

*Corresponding author.
e-mail: kishcha@hotmail.com

between simulated and observed dust loading (Tegen and Fung, 1995). The recently developed GOCART model, however, agrees in general with the presently available observations (Ginoux et al., 2001). Systematic errors in global climate models (GCMs) can be calculated instantaneously (e.g. as described in Machenhauer and Kirchner, 2000) or estimated by the analysis increments, which are the field differences between the analysis data and the model first guess. These increments include a complex combination of all kinds of model errors. Fortunately, these errors are strongly local, so they can be used as an indirect measure of specific atmospheric processes, which were not included in the model. In particular, these errors can be used for an analysis of the aerosol processes over regions where it is impossible to ignore the aerosol effects. This idea was successfully realized by Alpert et al. (1998) in their pioneering work over the east Atlantic Ocean and in subsequent studies (Alpert et al., 2000). They employed the analysis increments from the NASA GEOS-1 reanalysis over a 5-yr period to estimate the mean radiative forcing due to dust from the Sahara Desert. Now, however, the ERA increment data, which was received every 6 hr for 15 yr from 1979 to 1993, has become available to us. This provides further opportunity to investigate not only spatial distributions but also temporal changes of the dust effect on the climate, employing the ERA increments.

The dust is not the only contributor to model increments. Analysis errors, errors in the model resolved dynamics and errors in the parameterization of subgrid scale model processes may all contribute. It is believed that, in general, the parameterization of the various steps in the hydrological cycle, in particular cloud formation, and the parameterized cloud–radiation interactions are the main contributors to model errors (Christensen et al., 1998; Lau et al., 1995; Arking, 1991). However, over the Sahara desert during the pertinent period (April) such conditions are not predominant due to the low levels of relative humidity and cloudiness. On the contrary, the dust-forced heating/cooling of the atmosphere during that month and over the region under investigation is believed to be a predominant model defect which should affect significantly the increments. We want to consider just this dust effect. In this study this is achieved by considering correlation between the aerosol index and the increments, instead of considering the total increments.

2. Data and the procedure of analysis

The approach applied herein included a selection of appropriate regions for the investigation of dust effects, a suitable index of dust and a procedure of analysis.

The troposphere over the Sahara desert was chosen as a suitable region for our investigation. Prospero et al. (2001) and Israelevich et al. (2002) concluded that the atmosphere over North Africa is almost permanently loaded with a significant amount of mineral desert dust during the spring and the summer. They also showed that the region near the Chad basin is the most stable source of dust, with a maximum activity around April–May. Some other sources have their maximum activity in summer. Following their study, we focused our attention on the Sahara Desert in April, although the results for the other months were also analyzed.

2.1. Dust index

The dust distribution could be estimated by the TOMS aerosol index proposed by Herman et al. (1997). This index utilized the spectral contrast of two ultraviolet channels, 340 and 380 nm. It is positive for dust and proportional to the amount of the aerosol in the column along the line of sight. The TOMS AI index is an effective measure for dust mainly at altitudes higher than 1 km, and was proven to be effective in improving dust initialization for dust prediction models (Alpert et al., 2002).

It is worth noting some disagreement concerning the reliability of the AI calculation below 1 km. Herman et al. (1997) found that UV-absorbing aerosols in the boundary layer near the ground could not readily be detected by the method used for AI calculation. The cause was that near the ground the signal was relatively weak to the apparent noise from the ground. This means that the accuracy of AI is insufficient below 1 km, while above 1 km it is better. At the same time, Torres at al. (2002) consider that for mineral dust this restriction for TOMS AI is not so important and AI allows detection of dust particles even close to the ground.

Figure 1 (top panel) presents the two-dimensional (2D) distribution of the average value of the positive AI index for month of April between the years 1979–1993. Since the aerosol index is a measure of the column amount of aerosol, the local maxima of the AI distribution correspond to the strongest sources of

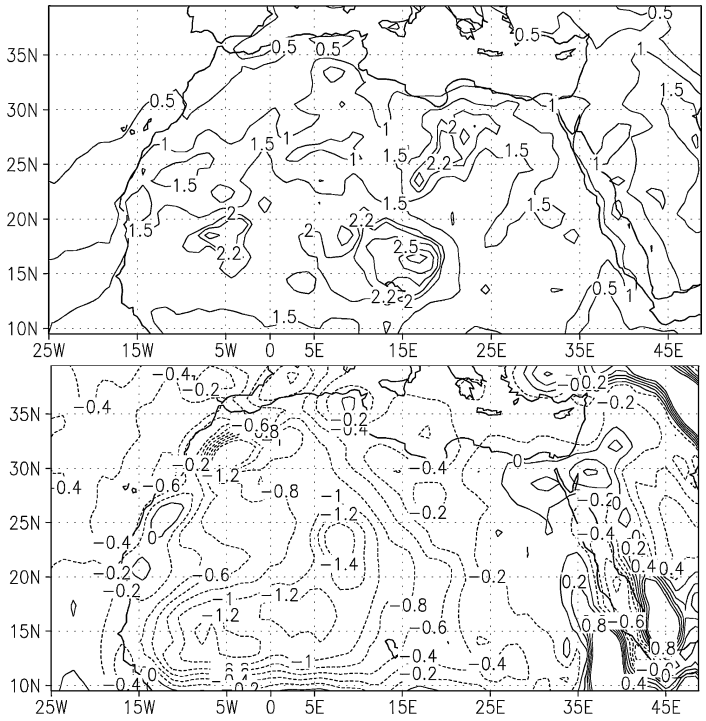

Fig. 1. The 2D distribution of the average value of positive AI index (top panel) and the ERA temperature increments at 12 UTC, at a pressure level of 775 hPa (bottom panel) for the month of April from 1979 to 1993.

aerosols. There are three main sources of dust over the Sahara Desert. The major source can be observed in the region (14°N–18°N, 12°E–18°E) around the Chad basin. Two smaller sources are located near the Atlantic coast (15°N–20°N, 3°W–8°W) and near the Mediterranean coast (24°N–28°N, 18°E–22°E). Yet another source of dust could be observed in the Arabian Peninsula. The dust sources estimated here are consistent with the analysis of Prospero et al. (2001) and Ginoux et al. (2001). They have shown that the sources can usually be associated with topographic lows, which have a deep accumulation of alluvial sediments composed of fine particles that are easily eroded by winds.

2.2. *Temperature increments*

The ECMWF Re-Analysis (ERA) project produced in 1994 a validated 15-yr data set of assimilated data for the period 1979–1993 (ERA Description). The data assimilation system employs the first guess, determined by a short-term forecast with a state-of-the-art GCM, together with all available observations as input for the analysis. These processes are repeated in a 6-h cyclic fashion.

The analysis increments (INC) used in the current study were defined as INC = AV − FGV, where AV are the analysis values and FGV are the 6-h first-guess forecast values. The FGV are determined by the GCM, which to a large extent ignore the dust processes. Strictly this is not true, since some constant aerosol radiative contribution was incorporated into the ERA model (Tanre et al., 1984). These estimations, however, do not account for large dust variability.

Thus, the INC are the values one should add to the FGV in order to get the AV. The 15-yr monthly and daily data of those temperature increments were employed in the current research.

The TOMS aerosol index is based on daytime measurements at about 8–9UTC. As such, it would be best to compare these indices with the daytime temperature increments. The 2D distribution of the increments for the month of April, at 12UTC and at a pressure level of 775 hPa is presented in Fig. 1 (bottom panel). This pressure level, as shown later, corresponds with the altitude of maximum correlation between the temporal

variations of AI and ERA increments. One can see high negative values over the Sahara Desert. The observed extreme zone of negative temperature increments does not coincide exactly with the AI index extreme zone. Hence, these increments seem not to be associated directly with the dust radiative forcing, but rather with some process of dust dynamics not included in the model. Obviously, the temperature increments might also depend on other processes, for example on errors in the modelling of vertical air motion.

2.3. *Procedure of analysis*

The main attention in this study was focused on the correlation analysis between temporal variations of the ERA increments and the AI indices. It should be noted that over the Sahara both the temperature increments and the aerosol index have very strong seasonal cycles with their maximum values in the same period, between April and July. To make the correlation relevant for supporting the link between dust and increments, these seasonal cycles should be eliminated. That was the reason why the correlated data sets were constructed for one selected month, i.e. every April, between 1979 and 1993. First, the increment data and necessary additional parameters from the ECMWF reanalysis data were interpolated into the grid of the AI index with a grid interval of 1° latitude and 1.25° longitude. Next, the correlation was calculated for temporal variations at every grid-point. Both monthly and daily data were used. The length of the correlated data sets for every grid-point was 15 and 450 points, for monthly and daily data, respectively.

3. Comparison of temporal variations

First, the monthly data are examined. In spite of the short length of comparable data sets for each grid-point the monthly data gives us an overview of the most interesting features. The correlation between the monthly average increments and AI in the daytime is shown in Fig. 2 (top panel). A distinctive structure is

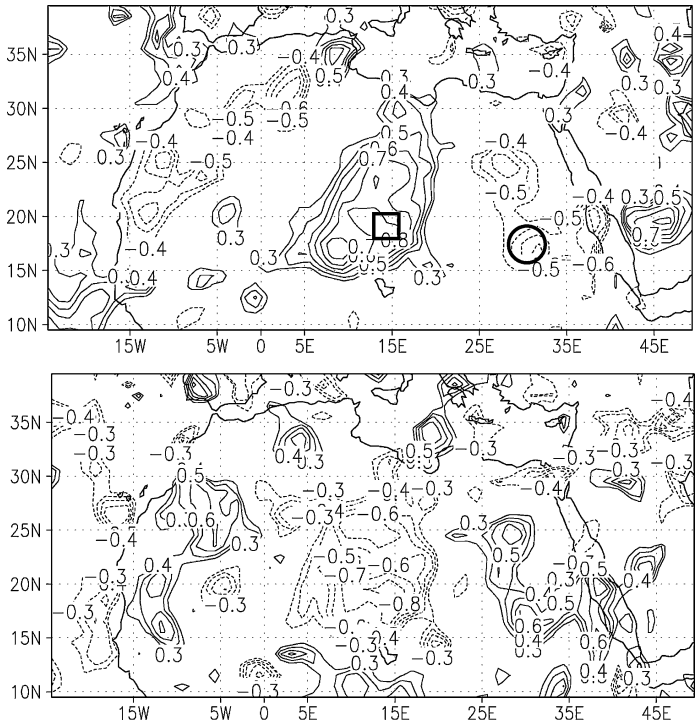

Fig. 2. Top panel: the field of correlation between the April temporal variations of positive AI index and temperature increments in the daytime, at 12 UTC, at pressure level 775 hPa from 1979 to 1993, monthly data. Bottom panel: the field of correlation between the temporal variations of lapse rate increments at pressure level 700–775 hPa and AI index. The square corresponds approximately to Domain 1 and the circle to Domain 2.

presented in the figure, composed of three areas. There is a big central area (15°N–30°N, 5°E–20°E) near the center of the Sahara Desert with a high positive correlation of more than 0.5. For some local maxima inside this area the correlation even exceeds 0.8. The whole high positive correlation area (PCA) is surrounded by an intermediate area of low correlation, between 0.3 and –0.3. An outermost high negative correlation area (NCA), less than –0.5, limits that intermediate area. The last area is not uniform, as it consists of a number of regions over the eastern and western parts of North Africa, with a relatively small amount of dust. It should be noted that another area of high positive correlation in the Arabian Peninsula could be seen as well.

This distinctive structure of correlation indicates the complex effect of desert dust on the climate. However, the question that arises here concerns the reliability of these results, which were based on monthly data sets for 15 points. A local significance of correlation for every grid-point was estimated, according to Fisher's test for small data sets (Wilks, 1955). It was presumed here that both the AI and the increments approximately follow the Gaussian distribution, taking into account negligible year-to-year connections. The testing process also included the test for field significance based on the Monte-Carlo approach (Livezey and Chen, 1983). The correlation r inside the maxima of PCA and NCA regions was found to be statistically significant within the 0.05 level when $|r| \geq 0.47$.

It is also interesting to examine the results for the longer (450 points) time series of daily data. In shifting to an analysis of daily data we should keep in mind the inconstancy of desert dust. The amount of dust in the atmosphere is a very variable parameter that depends strongly on wind, humidity and other parameters. The field of correlation between the daily AI indices and the increments does not show any significant correlation, neither positive nor negative. To separate systematic effects from casual ones the 15-d average data sets have been used. To eliminate seasonal cycles from consideration 15-d averages were also calculated for one selected month. The field of correlation between the 15-d averages of AI and INC shows the structure of correlation, which is similar to that found for monthly (30-d average) data sets. Comparing these two intervals of 15- and 30-d averaging showed that the longer the interval of averaging, the clearer the boundaries of the PCA and NCA areas.

4. Variations in the static instability over the Sahara

We assume that variations of the ERA temperature increments over the Sahara desert are due mainly to the dust-forced heating/cooling. This dust forcing may also be responsible for the variations of static instability inside the dust layer. It was shown by Karyampudi et al. (1999) on the basis on lidar observations that the Saharan dust layer is less stable and close to the adiabatic layer at 850–500 hPa than its two limiting inversion layers. The same structure of temperature stratification was also estimated by Hsu et al. (1999). However, it is difficult to determine the lapse rate change, which is due to the dust effect alone. Fortunately, the ERA temperature increments do provide us with the opportunity to estimate the contribution.

According to the definition of the increments, they indicate the difference between the analysis and the first guess of the climate model, ignoring dust processes within the data assimilation system. Hence, the vertical gradient of the temperature increment in every grid-point is approximately the difference between the real lapse rate in the presence of dust, and the lapse rate under conditions of no dust. This vertical gradient of the temperature increment will be called as the "lapse rate increment." The value of the average lapse rate increments $\gamma_{\mathrm{INC}} = [\mathrm{d(INC)}/\mathrm{d}Z]_{p_i, p_{i-1}}$ between two fixed adjacent pressure levels $p_i < p_{i-1}$ could be estimated as follows:

$$\gamma_{\mathrm{INC}} = (\mathrm{INC}_{p_i} - \mathrm{INC}_{p_{i-1}})/(Z_{p_i} - Z_{p_{i-1}})$$

whereas $\mathrm{INC}_{p_i}, \mathrm{INC}_{p_{i-1}}$ are temperature increments (monthly means) at pressure levels p_i, p_{i-1} and $Z_{p_i}, Z_{p_{i-1}}$ are the geopotential heights of the same pressure levels. These geopotential heights were taken from the ECMWF reanalysis monthly mean pressure level data.

The correlation analysis between the temporal variations of the lapse rate increments and the AI indices was done using by the same approach we employed for the temperature increments. Figure 2 (bottom panel) shows the correlation map between the lapse rate increments in the layer from 700 to 775 hPa and AI, at 12 UTC. A distinctive structure can be seen, resembling a mirror image of the structure shown in Fig. 2 (top panel). There is a large area near the center of the Sahara desert with a high negative correlation levels from –0.8 to –0.5 (denoted NCA-γ). An intermediate area of low correlation surrounds the NCA-γ area.

Table 1. *Correlation* r *and parameters* (a, b) *of the linear regressions between AI indices, temperature increments (INC), and lapse rate increments* γ_{INC} *for domains 1 and 2*

	Domain 1			Domain 2		
Linear regression	r	a	b	r	a	b
$\mathrm{INC} = a + b \times \mathrm{AI}$	0.66	−1.5647 (K)	0.3159 (K)	−0.53	0.7516 (K)	−0.7759 (K)
$\gamma_{\mathrm{INC}} = a + b \times \mathrm{AI}$	−0.62	0.9769 (K/km)	−0.2644 (K/km)	0.50	−0.3984 (K/km)	0.4719 (K/km)
$\gamma_{\mathrm{INC}} = a + b \times \mathrm{INC}$	−0.78	−0.2058 (K/km)	−0.6992 (km^{-1})	−0.73	0.0770 (K/km)	−0.4746 (km^{-1})

An outermost area with a high positive correlation of more than 0.5 (denoted PCA-γ) limits that intermediate area.

To better understand the previous figures, let us examine the next two scatterplots (Fig. 3), which show the relationship between monthly values of AI indices and both the temperature increments at the altitude of correlation maximum and the lapse rate increments at above the height of correlation maximum. These scatterplots present us with points for two domains with different signs of correlation: Domain 1 (18°N–20°N, 14°E–16°E) and Domain 2 (16°N–18°N, 30°N–32°E), already used above. It can be seen that when the AI increases from 0.5 to 1.5 the increment decreases, while the lapse rate increment increases. Consequently, in the domain with low AI levels, the dust layer becomes cooler and the atmosphere above this layer will be more stable. However, when the AI increases from 1.5 to 3.5, the increment progressively increases but the lapse rate increment decreases. Hence, in the domain with high AI exceeding 1.5, the dust layer becomes warmer and the atmosphere above the layer would be less stable. The scatterplots clearly show that the chosen PCA and NCA regions are two distinct domains with almost no overlap of their INC values [and only some overlap of d(INC)/dZ].

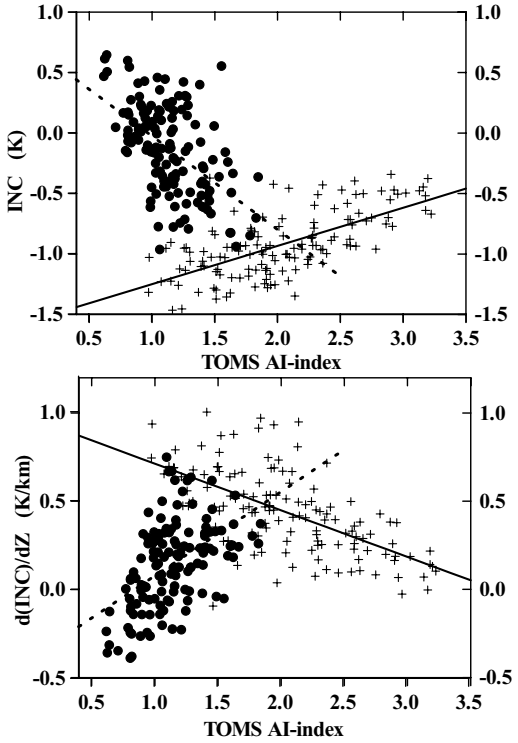

Fig. 3. Top panel: scatterplot between the daytime temperature increments at 775 hPa and AI indices. Bottom panel: scatterplot between the lapse rate increments at 700–775 hPa and AI indices for the month of April in the years from 1979 to 1993. These scatterplots are joined for domains 1 (crosses) and 2 (circles). Solid and dotted lines correspond to linear regressions.

Within both domains 1 and 2, the relationship between the AI indices, INC, and γ_{INC} can be quite accurately estimated using linear regressions. The parameters of the linear regressions are presented in Table 1. Each of these linear dependencies was based on 135 pairs of points. These pairs were taken for nine grid-points located inside the selected domain over a period of 15 yr from 1979 to 1993. The correlation is also presented in Table 1. It is statistically significant at the 0.05 level. According to the computed linear regression, the average response of air temperature to dust at 775 hPa in Domain 1 was estimated at about 0.3 K per AI unit.

5. The vertical structure of correlation

The vertical structure of correlation between the AI index and temperature increments has been examined using the vertical correlation profiles for two small

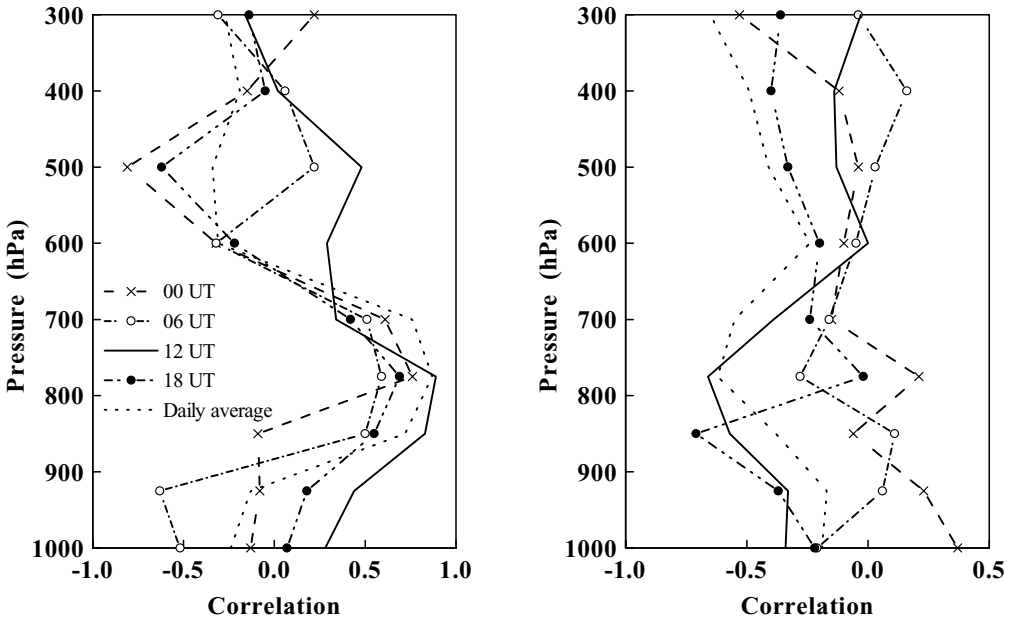

Fig. 4. The vertical profiles of correlation between the AI index and temperature increments for four specific times of the day (00, 06, 12 and 18 UTC) in addition to daily average increments. The left panel corresponds to domain 1 (18°N–20°N, 14°E–16°E) inside the PCA area, and the right panel corresponds to domain 2 (16°N–18°N, 30°E–32°E) inside the NCA area.

domains inside the PCA and the NCA: Domain 1 (18°N–20°N, 14°E–16°E) and Domain 2 (16°N–18°N, 30°E–32°E) correspondingly (Fig. 4). Five correlation profiles for the temperature increments during four different times of day (00, 06, 12 and 18 UTC), as well as for the daily average increments, were plotted into one graph. This illustrates the variability of the dust effect, as compared to the solar effect. It should be emphasized that monthly values of INC for these four different times of day and their average have been used for correlation profiles together with monthly AI data.

For the PCA, the high correlation (>0.5) occurs at pressure levels from 700 to 850 hPa for all times of day (Fig. 4, left panel). This means that in this layer over the area of maximum dust concentration, the dust effect dominates. The daily layer of high correlation descends slightly to levels from 775 to 850 hPa. At night, it goes up from 700 to 775 hPa. At level of 500 hPa there is a low positive correlation during the daytime and high negative correlation at night. For all correlation profiles for PCA the peak is at about 775 hPa in April.

For the NCA only the solar effect is visible (Fig. 4, right panel). In this area the AI indices are small, often less than 1. At the same time it can be noted that the daytime highest negative correlation is again at 775 hPa as for the PCA.

6. Distinctions between large-scale synoptic patterns over the areas with positive and negative correlation

The distinctive structure of correlation, described above, points to the significant local atmospheric response to dust variations. However, on a large scale it is known that the dust distribution, emission, transport and deposition are determined by atmospheric dynamics (Ginoux et al., 2001). One would expect to find some distinction between large-scale synoptic patterns over the PCA and NCA areas. These large-scale synoptic patterns were examined employing the ERA reanalysis data for the month of April, during the period in question.

As an example, Fig. 5 shows the 2D distribution of average values of wind vectors (top panel), vorticity (middle panel) and relative humidity (bottom panel) at the pressure level of 775 hPa for the month of April,

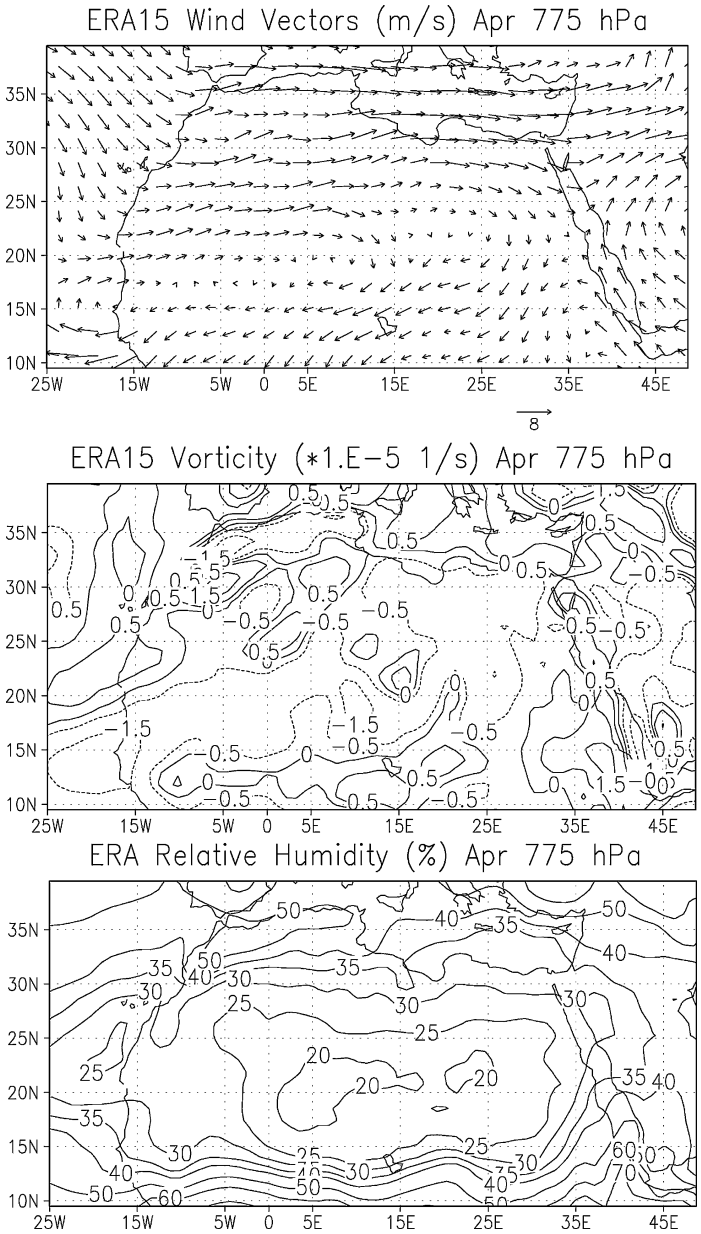

Fig. 5. The 2D distribution of the average wind vectors (top panel), the average value of vorticity (middle panel) and the average value of relative humidity (bottom panel) for the month of April in the years from 1979 to 1993 at the pressure level 775 hPa. The ERA15 reanalysis data were used.

derived from the ERA reanalysis data. One can see that an anticyclonic flow prevails in the PCA area and a cyclonic flow in the NCA areas. It should be noted that an anticyclonic flow takes also place over the desert in the Arabian Peninsula. At the same time, a cyclonic flow in NCA is not as obvious as the anticyclonic one in PCA.

The negative vorticity corresponds mostly to the PCA area, while the positive vorticity to the NCA areas. The relationship between the field of correlation

r(AI indices & increments) and the field of vorticity becomes more significant under higher thresholds of r, for example when the threshold is $|r| > 0.5$. It is interesting that negative vorticity over the PCA is observed at all tropospheric heights higher than 775 hPa. The above findings point to the specific role of vertical air motion in the atmospheric temperature response to the dust effect.

In the region in question, in spring and in summer, large-scale vertical air motion is primarily defined by the northward shifting of the Intertropical Convergent Zone (ITCZ). In order to gain further information about the relationship between the air motion and the dust effect over the PCA/NCA, latitudinal cross-sections, zonally averaged over these regions, were analyzed. V and W wind components were used to construct the streamlines for the April latitudinal cross-sections. Vertical velocity was multiplied by 1000 to be in agreement with the ratio of the horizontal to the vertical scale of the troposphere. Figure 6 (top panel), corresponding to the cross-section over the PCA, shows the well known Hadley's cell: an upward airflow inside ITCZ near the equator surrounded by a downward flow on the North and on the South. We see that the PCA is crossed prominently by the downward streamlines. When this cross-section of streamlines is compared with that of the aerosol index (Fig. 6, top and bottom panels) one can see that the PCA does not coincide with the latitudinal interval of the dust maximum but is somewhat shifted to the northward direction. In its turn, the NCA is crossed mainly by the upward airflow, which is not as obvious as in the PCA.

7. Discussion

A number of qualitative arguments are presented herein, to explain the April correlation results.

7.1. PCA case

The first case, relevant for the relatively thick dust layers in the PCA, is associated primarily with direct solar heating of the dust layer due to absorption of short-wave (solar) radiation in the dust layer. The main daytime solar radiation comes from above, but a part of it is backscattered short-wave radiation and some other part is short-wave radiation reflected from the surface. Part of the solar radiation is absorbed in the dust layer and heats it. Such solar heating of the dust layer would most probably increase with the thickness of the layer, until the layer (if possible) reaches a certain thickness and becomes impenetrable. In this case the heating of the surface by solar radiation is negligible and, as a result, long-wave heating due to absorption of thermal

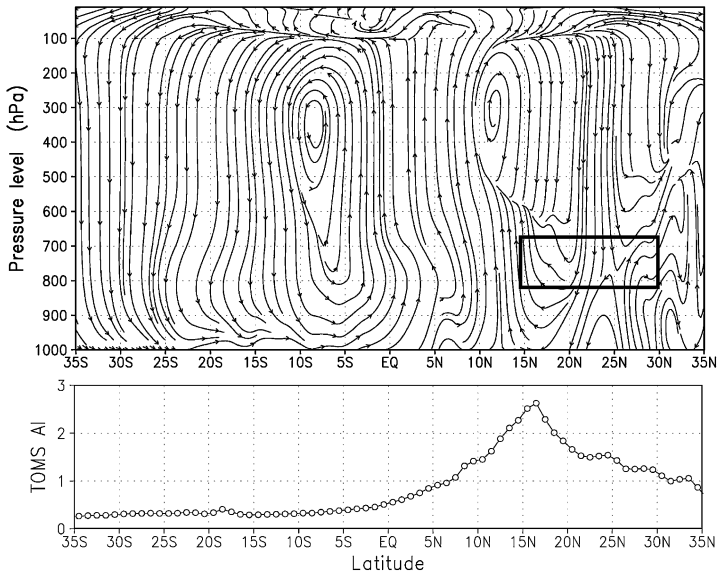

Fig. 6. The field of streamlines for the latitudinal cross-section, zonally averaged over the PCA in the month of April, is shown in the top panel. The rectangle corresponds to the PCA. The bottom panel presents the latitudinal cross-section of TOMS AI.

radiation from the surface also becomes negligible, or even negative. In this case, only the direct solar heating from above is relevant, resulting in stabilization of the dust layer. At night the top of the dust layer is temporarily cooled by long-wave radiation to space, but in daytime solar heating will dominate.

7.2. NCA case

The second case, relevant for relatively thin dust layers, is primarily associated with heating/cooling due to absorption/emission of long-wave (thermal) radiation. At night, net long-wave radiation from the top of the layer into space leads to a cooling of the dust layer. As a result the layer is destabilized. In daytime the absorption of solar radiation in the top of the dust layer counteracts the long-wave cooling there and the destabilization. However, at the same time the solar radiation, which penetrates the thin dust layer, heats the surface, which in turn heats the dust layer by long-wave radiation from below with destabilization as a result. The daytime surface temperature reached is, however, reduced with the increasing thickness of the dust layer, due to increasing backscattering and absorption of short-wave (solar) radiation by the dust layer. As long as the daytime surface temperature remains higher than that of the dust layer, additional turbulent heat transfer from the surface to the dust layer will take place, and the static instability of the layer will enhance the turbulent mixing. As the turbulence develops, the lapse rate in the dust layer will approach the dry adiabatic value. At night, the surface temperature, due to the net upward long-wave radiation from the surface, falls below that of the dust layer. This surface cooling also decreases with the increasing of the thickness of the dust layer. It causes cooling of the dust layer from below and tends temporarily to stabilize the dust layer. However, the daytime heating and destabilization from below will dominate. Thus, for the thin dust layers in the NCA, these mechanisms may explain the decreasing heating combined with the increasing AI. For thicker dust layers the daily surface temperature variation becomes smaller, and consequently the long-wave heating from below will also diminish. Instead, for dust layers with thickness above a certain value, the first (short-wave) type of radiative heating from above becomes dominant.

As presented in Fig. 3 (top panel), in the NCA domain the temperature increments decrease as the AI increases. The explanation for this fact is that in the NCA domain the dust layers are thin, therefore the long-wave heating from below, which decreases due to the increasing thickness of the layer, dominates the direct solar heating from above. On the other hand in the PCA domain the dust layer is relatively thick, and therefore the direct solar heating from above, which increases with thickness, dominates the long-wave heating from below. This explains why the PCA temperature increments in Fig. 3 (top panel) increase as the AI increases.

In accordance with Fig. 3 (bottom panel), one can assume that the top of the dense dust layer is at 775 hPa both in the NCA and the PCA regions. The results in Fig. 4 indicate that this is the case on average. Above that level, the dust concentration should reach zero, and at 700 hPa the temperature increments due to the dust should reach values close to zero. Again, Fig. 4 indicates that this is the case. Thus, approximately $-[\mathrm{d(INC)}/\mathrm{d}Z]$should be proportional to INC. Therefore, in the NCA cases, $[\mathrm{d(INC)}/\mathrm{d}Z]$ should increase with increasing AI, while INC decreases as AI increases. In the PCA cases, $[\mathrm{d(INC)}/\mathrm{d}Z]$ should decrease as AI increases, while INC increases.

It is interesting to compare the vertical distribution of correlation found here with that of Saharan dust concentrations. On the one hand, in accordance with Hsu et al. (1999), the average height of the dust layer was also approximately 800 hPa, as measured over Dakar, Senegal, on the edge of the dust region, in spring. On the other hand, the aerosol backscattering measurements during the Lidar in Space Technology Experiment (LITE) showed that dust concentrations maximized at the surface close to the dust source in the Western Sahara (Ginoux et al., 2001). Of course, the dust source in the Western Sahara and the one under discussion over the Chad basin are not identical. Nevertheless, it seems reasonable to assume that dust always maximizes at the surface near the dust source. We can see the same disagreement concerning the altitude the dust can reach. Hsu et al. (1999) found it was 700 hPa, while according to LITE data the dust plume extended to 5 km. Thus, there seems to be no simple relation between the correlation profiles and the vertical distribution of dust concentrations.

The above explanations are based just on a 1D examination of radiative transfer. It ignores the facts that the PCA (NCA) area is mostly anticyclonic (cyclonic) and also that PCA is shifted to the northward direction relative to the dust maximum. This evident effect of atmospheric circulation suggests that the temperature increments can be due to not only radiative dust processes missing in the model but also due to errors

in the modelling of air motion near the ITCZ. In accordance with the findings of Miller and Tegen (1998), the radiation effect of dust differs in regions with deep convection and with subsidence. It is quite possible to assume that in our case the dust presence in the region in question results in the dust-forced heating/cooling, modulated by overlap of convection and subsidence processes. In such a manner the dust effects are incorporated into the temperature increments. This assumption permits us to explain the distinctive structure of correlation between AI and INC and the relationship between the correlation and air motion.

The fact that the PCA (NCA) is crossed by downward (upward) airflow indicates a possible dynamic interaction between the presence of dust and the synoptic systems. In other words, it seems possible that dust works to change the dynamic–synoptic systems in which it acts. Both the upward and downward air motion may be changed in the presence of dust, causing additional adiabatic cooling/warming. It should be stressed that this possibility still require verification.

One point that needs clarification is the absorption of radiation by dust. Kaufman et al. (2001) showed that absorption of sunlight by dust from Africa over the Atlantic Ocean is significantly lower than presently measured in situ. The single scattering albedo at the wavelength of 0.64 μm was found to be about 0.97, as opposed to 0.87 in previous measurements. As discussed above, the dust-forced heating in the PCA is associated mainly with the dust absorption of sunlight. One possible explanation for this discrepancy may be the multiple reflections occurring in the dust layer as well as between the surface and the dust layer. Another explanation may be that the thermal radiation emitted from the earth's surface is responsible for part of the heating.

Another important question concerns the role of humidity and moist air in atmospheric model errors over anticyclonic and cyclonic areas mentioned in the Introduction. Figure 5 (bottom panel) shows the 2D distribution of the average relative humidity values at the pressure level of 775 hPa, taken from the ERA reanalysis data. In April the relative humidity is about 20% in the PCA and about 30–40% in the NCA. Our analysis of the ISCCP data for cloudiness for the period from 1983 to 1990 shows that for the month of April, the total cloud coverage is 20–25% in the PCA and 30–35% in the NCA. This means that the atmosphere in the PCA is drier and the effect of humidity (and cloudiness) is less significant there. This is consistent with the downward airflow found in the PCA. It is evident that in the NCA increased humidity and cloudiness should accompany the upward airflow. It is also worth noting that in the NCA aerosol indices are small, often less than 1. Therefore, here we can not be positive that the temperature increments are influenced mainly by dust.

In accordance with the latter paragraph, our choice of the month of April for the analysis was justified by its appropriate atmospheric conditions: low levels of humidity/cloudiness and a high level of dust activity near Lake Chad. Thereby the low impact of moist air on the increments is associated with the significant dust effect. The same correlation analysis was also conducted for all months of year. It was found that the PCA takes place from April to July, during the period of maximum dust activity, in the vicinity of the dust source near Lake Chad. The PCA is less pronounced when compared to April, and it does not follow the shift of the major dust maximum from the Lake Chad basin to the west part of the Sahara Desert. In August the PCA disappears. The analysis of radiative forcing of desert dust for other months except April is more complicated because of the increase in humidity and its impact on the increments. As an example, annual variations of relative humidity, averaged from 1979 to 1993 within the region (15°N–20°N, 10°E–20°E) around Lake Chad, together with its standard deviations, are presented in Table 2. Over the period from April to August relative humidity increased more than double, from 22.0 to 50.9%. This result can be

Table 2. *Annual variations of relative humidity* (RH)*, averaged from 1979 to 1993 within the region (15°N–20°N, 10°E–20°E) around Lake Chad, and standard deviation* (SD) *of its year-to-year changes*[a]

Month	RH (%)	SD (%)
01	17.0	4.7
02	18.6	2.8
03	18.6	2.8
04	21.9	3.3
05	30.8	9.4
06	32.2	7.7
07	45.8	9.3
08	50.9	11.2
09	38.3	6.1
10	27.3	3.4
11	24.0	5.1
12	18.4	3.7

[a]The ERA15 reanalysis monthly data at pressure level of 775 hPa were used.

associated with the northward progress of the ITCZ in summer (website: http://www.cpc.ncep.nasa.gov/products/african_desk/ITCZ). The latter process is accompanied, on the one hand, by the increasing impact of moist air on the increments, and, on the other hand, by decreasing the dust activity near Lake Chad. Moreover, the standard deviation of year-to-year-changes in relative humidity also increased over the period from April to August, from 3.3 to 11.2%, respectively (Table 2). It is worth noting that already in May the standard deviation was 9.4%. This process results in a decrease in the correlation between the increments and dust. Therefore the atmospheric conditions in summer are not so suitable for looking at the radiative effect of desert dust from the increments. In winter, a low level of dust activity can be observed near Lake Chad, so the winter period is also not suitable for our purpose. Hence, in accordance with all aforementioned facts April was considered as the most suitable month for this study.

An important support for the April results was obtained from the analysis of vertical distribution of dust concentration derived from the 24-h dust prediction system at Tel Aviv University (Alpert et al., 2002) (website: http://earth.nasa.proj.ac.il/dust/current/). The vertical distribution of correlation between AI and the ERA over the Lake Chad basin was found to be in agreement with the modeled dust concentration in April. These results are in preparation for publication.

8. Conclusions

This study looks at the radiative effect of desert dust through the ERA temperature increments. These increments result from many kinds of model errors and not only from radiative dust processes missing in the model. Over the Sahara desert the dust radiative effect is believed to be a predominant model defect which significantly affects the increments. This dust effect was examined by considering the time correlation between the increments and remotely sensed dust. As is well known, correlation does not indicate causation and is only consistent with causation. Nevertheless, we consider that the analysis of spatial distribution of correlation expands our knowledge of dust effects. As is evident from the foregoing the correlation analysis indeed gives us the opportunity to determine the following main features of the relationship between the AI and the temperature increments in the month of April:

First, a distinctive structure was identified in the distribution of correlation composed of three nested areas with high positive correlation (>0.5), low correlation and high negative correlation (< -0.5) correspondingly.

Next, the high positive correlation over the main dust maxima near the Chad basin takes place at the pressure levels from 700 to 850 hPa, with the highest value at a pressure level of 775 hPa. The dust effect in the PCA is more significant than the solar effect in the correlation vertical profiles at all times of day. It is accompanied by a decrease in the static stability of the atmosphere above the dust layer.

Finally, the PCA (NCA) corresponds mainly to anticyclonic (cyclonic) flow, negative (positive) vorticity and downward (upward) airflow. These facts indicate an interaction between dust-forced heating/cooling and atmospheric circulation.

For other months except April the analysis of radiative forcing of desert dust is more complicated because of the increase in humidity and its impact on the increments. Further investigation is required to establish the role of different contributing factors to the increments.

9. Acknowledgments

We appreciate the constructive remarks and suggestions made by Dr. Y. Kaufman, B. Starobinez and Dr. S. Yang. We thank the two anonymous reviewers for their positive criticism and very fruitful comments. This research was supported by the EU DETECT Project, Contract No. EVK2-CT-1999-00048.

REFERENCES

Alpert, P., Kaufman, Y. J., Shay-El, Y., Tanre, D., da Silva, A., Schubert, S. and Joseph, J. H. 1998. Quantification of dust-forced heating of the lower troposphere. *Nature* **395**, 367–370.

Alpert, P., Herman, J., Kaufman, Y. J. and Carmona, I. 2000. Response of the climatic temperature to dust forcing, inferred from total ozone mapping spectrometer (TOMS) aerosol index and the NASA assimilation model. *Atmos. Res.* **53**, 3–14.

Alpert, P., Krichak, S. O., Tsidulko, M., Shafir, H. and Joseph, J. H. 2002. A dust prediction system with TOMS initialization. *Mon. Weather Rev.* **130**, 2335–2345.

Christensen, O. B., Christensen, J. H., Machenhauer, B., and Botzet, M. 1998. Very high-resolution regional climate simulations over Scandinavia – present climate. *J. Climate* **11**, 3204–3229.

Arking, A. 1991. The radiative effects of clouds and their impact on climate. *Bull. Am. Meteorol. Soc.* **72**, 795–813.

Ginoux, P., Chin, M., Tegen, I., Prospero, J. M., Holben, B., Dubovik, O. and Lin, S.-J. 2001. Sources and distributions of dust aerosols simulated with the GOCART model. *J. Geophys. Res.* **106**, 20 255–20 274.

Gobbi, G. P., Barnaba, F., Giorgi, R. and Santacasa, A. 2000. Altitude-resolved properties of a Saharan dust event over the Mediterranean. *Atmos. Environ.* **34**, 5119–5127.

Hamonou, E., Chazette, P., Balis, D., Dulac, F., Scheider, X., Galani, E., Ancellet, G. and Papayannos, A. 1999. Characterization of the vertical structure of Saharan dust export to the Mediterranean basin. *J. Geophys. Res*. **104**, 22 257–22 270.

Herman, J. R., Bhartia, P. K., Torres, O., Hsu, C., Seftor, C. and Celarier, E. 1997. Global distribution of UV-absorbing aerosol from Nimbus-7/TOMS data. *J. Geophys. Res.* **102**, 16 911–16 922.

Hsu, N. C., Herman, J. R., Torres, O., Holben, B. N., Tanre, D., Eck, T. F., Smirnov, A., Chatenet, B. and Lavenu, F. 1999. Comparisons of the TOMS aerosol index with Sun-photometer aerosol optical thickness: results and applications. *J. Geophys. Res.* **104**, 6269–6279.

Israelevich, P. L., Levin, Z., Joseph, J. H. and Ganor, E. 2002. Desert aerosol transport in the Mediterranean region as inferred from the TOMS aerosol index. *J. Geophys. Res.,* in press.

Karyampudi, V. M., Palm, S. P., Reagen, J. A., Fang Hui, Grant, W. B., Hoff, R. M., Mouline H. R., Pierce, H. F., Torres, O., Browell, E. D. and Melfi, S. H. 1999. Validation of the Saharan dust plume conceptual model using lidar, Meteosat, and ECMWF data. *Bull. Am. Meteorol. Soc.* **80**, 1045–1075.

Kaufman, Y. J., Tanre, D., Dubovik, O., Karnieli, A. and Remer, L. A. 2001. Absorption of sunlight by dust as inferred from satellite and ground-based remote sensing. *Geophys. Res. Lett.* **28**, 1479–1482.

Kaufman, Y. J., Tanre, D. and Boucher, O. 2002. A satellite view of aerosols in the climate system. *Nature* **419**, 215–223.

Lau, W. K., Sud, Y. C. and Kim J. H. 1995. Intercomparison of hydrologic processes in global climate models. NASA Technical Memorandum 104 617.

Livezey, R. and Chen, W. Y. 1983. Statistical field significance and its determination by monte-carlo techniques. *Mon. Weather Rev.* **111**, 46–59.

Machenhauer, B. and Kirchner, I. 2000. Diagnosis of systematic initial tendency errors in the ECHAM AGCM using slow normal mode data assimilation of ECMWF reanalysis data. *CLIVAR Exchanges* **5**, 9–10.

Miller, R. L. and Tegen, I. 1998. Climate response to soil dust aerosols. *J. Climate* **11**, 3247–3267.

Prospero, J. M., Ginoux, P., Torres, O., Nicholson, S. and Gill, E. 2002. Environmental characterization of global sources of atmospheric soil dust identified with the NIMBUS-7 total ozone mapping spectrometer (TOMS) absorbing aerosol product. *Rev. Geophys.*, **40**, 1002, doi:10.1029/2000RG000095.

Tanre, D., Geleyn, J. F. and Slingo, J. 1984. First results of the introduction of an advanced aerosol-radiation interaction in the ECMWF low resolution global model. In: *Aerosols and their climatic effects*. (eds. H. E. Gerber and A. Deepak), Publisher? Place? 133–177.

Tegen, I. and Fung, I. 1995. Contribution to the atmospheric mineral aerosol load from land surface modification. *J. Geophys. Res.* **100**, 18 707–18 726.

Torres, O., Bhartia, P. K., Herman, J. R., Sinyuk, A., Ginoux, P. and Holben, B. 2002. A long-term record of aerosol optical depth from TOMS observations and comparison to AERONET Measurements. *J. Atmos. Sci.* **59**, 398–413.

Wilks, D. S. 1995. *Statistical methods in the atmospheric sciences: an introduction*. Academic Press, New York, 467 pp.